Microstructure and Corrosion Properties of Ti-6Al-4V alloy by Ultrasonic Shot Peening

Conghui Zhang[*], Wei Song, Fengbo Li, Xu Zhao, Yaomian Wang, Guizhi Xiao

School of metallurgical engineering, Xi'an University of Architecture and Technology, Xi'an, Shaanxi 710055, China
[*]E-mail: jiandazhang2010@hotmail.com

A nanostructured surface layer of Ti-6Al-4V alloy was obtained through ultrasonic shot peening (USSP). The microstructure and microhardness were studied using an optical microscope and a nanoindentation tester. The corrosion performance of the Ti-6Al-4V alloy was investigated using potentiodynamic polarization and electrochemical impedance spectroscopy (EIS). The composition of the passive film formed on the surface was analyzed using X-ray photoelectron spectroscopy (XPS). The results show that the grain size of the surface layer is on nanometer scale and increases gradually from the surface to the matrix after USSP treatment. The surface microhardness reaches up to approximately 7 GPa, which is significantly higher than that of the matrix. The self-corrosion potential of the USSP samples increases compared with that of the untreated sample, and the corrosion current density decreases by two orders of magnitude, the capacitive resistance is much larger. A compact and stable passive film forms on the surface after USSP treatment. High-density nanograin boundaries and dislocations generated from surface nanocrystallization provide more channels for Ti^{4+} to form passive oxide films.

1. INTRODUCTION

Titanium and Ti alloys are widely used in aerospace, navigation, and dental implants because of their low density, excellent mechanical properties, and biocompatibility. The passive films formed on the titanium and its alloys enhance corrosion resistance. However, Ti alloys still frequently encounter failure when applied, and most failures, including stress fracture, wear, and corrosion, occur on the surface of the materials. Therefore, strengthening the surface properties has a great significance in improving the overall behavior of Ti alloys.

USSP treatment uses high-frequency projectile impacting specimen surface repeatedly to achieve grain refinement and introduce the compressive residual stress at the same time. USSP treatment could significantly improve the mechanical properties of materials. Wu et al.[1] reported that a strengthened layer was produced on the surface after USSP treatment. The mechanism of grain refinement has been discussed as well. Unal et al.[2] reported that the nanohardness after USSP was approximately 1.5 times higher than that of the initial state, and the elastic modulus increased to approximately two times that of the initial state. Mao et al.[3] reported that USSP treatment enhanced the wear and corrosive wear resistance of Cu-30 Ni alloys. The nano-sized grains obtained during the USSP treatment were considered as the major factor in enhancing wear and corrosive wear resistance.

The factors influencing corrosion behavior are complex, and the results obtained by different authors are controversial. The four major factors are described as follows. (1) Grain size is a critical factor in the corrosion resistance of metallic materials. Wang et al.[4] investigated the effect of surface nanocystallization induced by shot peening on the corrosion resistance of 1Cr18Ni9Ti stainless steel. They pointed that surface nanocrystallization decreased the current density and improved the corrosion resistance of stainless steel. (2) Compressive residual stress is another factor in increasing corrosion resistance. Trdan et al.[5] reported that a significant improvement in pitting potential was observed in 0.05 M NaCl solution after pure mechanical laser peening on AA6082-T651 Al alloy. They pointed that the increase in critical pitting potential was attributed to the effects of compressive residual stress and work hardening. Liu et al.[6] confirmed the beneficial effects of compressive stress on localized corrosion. The samples with compressive residual stress increased the breakdown and repassivation potentials and decreased the passive current density. (3) Roughness is also an important factor in corrosion resistance. Lee et al.[7] studied the influence of surface roughness on the corrosion behavior and showed that smoother surface indicated better corrosion resistance. The surface active area became larger and the corrosion rate became faster with the increase in surface roughness. (4) The processing method degree[8], and corrosion environment[9-11] are also the influencing factors in corrosion resistance.

The corrosion resistance of Ti and its alloys has been extensively studied. Balyanov et al.[12] found that Equal channel angular pressing derived ultrafine-grained Ti could more readily form passive film on the surface than coarse-grained Ti, and the impurity segregation was more homogeneous than in coarse-grained Ti. Johansen et al.[13] had a similar viewpoint, and they pointed that passivation initially started on the crystalline lattice defects of the surface. This effect could be avoided by the adsorption of albumin onto the metal surface. Huang et al.[10] reported that the passive films formed on Ti-6Al-4V alloy could be destroyed by fluoride ions via Na_2TiF_6 formation when the NaF concentration was increased to 0.1%. Ittah et al.[14] reported that the pitting sensitivity of titanium in different density of corrosion medium was anomalous. Furthermore, Silva et al.[15] reported that nitrogen enriched Ti-6Al-4V alloy layer was formed on the material surface through plasma-immersion ion implantation, which resulted in better corrosion resistance for Ti-6Al-4V alloy.

Nevertheless, the relationship between the microstructure and corrosion properties of Ti-6Al-4V alloys is unclear. This study aims to explore the relationship between microstructure and corrosion properties (in 3.5% NaCl) of Ti-6Al-4V before and after USSP.

2. EXPERIMENTAL

2.1. Materials

Commercial titanium alloy(Ti-6Al-4V) was selected for USSP treatment. The samples were ground and washed with acetone, and then dried in air before USSP. The ZG30 pill with 3mm diameter was jetted at a constant angle for 85°under 0.4 MPa working pressure. The samples were subjected to USSP treatment for 15, 30, and 45 min, respectively.

The corrosion specimens were cut from USSP treatment plate in a dimensions of 15 mm ×15 mm ×4 mm. After being washed with acetone, specimens were embedded in epoxy resin with a top surface exposed area of 1 cm^2.

2.2. Methods

The OLYMPUS GX51 was used to observe the microstructure. Nanoindentation test was performed by Agilent Nano Indenter G200. The test started from the top surface to the matrix, 20 μm as an interval, and it was kept at the maximum load of 5 gf for 10 s. The JEM-3010 transmission electron microscopy was used to observe the microstructure of the sample.

Electrochemical experiments were performed by PARSTAT-4000, equipped with a standard three-electrode configuration: using a platinum sheet as auxiliary electrode and a saturated calomel electrode (SCE) as the reference electrode. The corrosion medium is 3.5% NaCl solution. Before the electrochemical test, the specimens were immersed in the solution for 30 min for the equilibrium potential. In order to clarify the reproducibility, the tests were repeated three times. Potentiodynamic polarization curves were performed in the potential range from -250 mV to 800 mV at a scan rate for 1.5 mV/s. EIS experiments were realized in the frequency range from 100 KHz–0.01 Hz with AC amplitude of ±10 mV superimposed to the open circuit potential value[16]. Both the experiments and the data were fitted using the ZSimpWin software. Surface chemical compositions of both untreated and 30 min USSP-treated sample, which were immersed in 3.5% NaCl solution at room temperature for one month, were analyzed by X-ray photoelectron spectroscopy (XPS). The XPS were performed in an K-Alpha spectrometer with a monochromatic Al Kα X-ray source of 1486.71 eV and a power of 225W. The binding energy was calibrated with C1s peak with a binding energy value of 284.8 eV.

3. RESULTS AND ANALYSIS

3.1. Microstructure

The microstructure of cross-sectional Ti-6Al-4V specimens after USSP is shown in Fig.1. The bright contrast α phase and dark contrast β phase are homogenously distributed in the specimen. The grain in the surface region is fragmented, and the grain boundary cannot be distinguished. The change in grain orientation is confirmed by the elongated microstructure near the surface. The matrix is approximately isometric crystal. The thickness of severe plastic deformation layer with the processing

time of 15, 30, and 45 min is about 100, 150, and 170 μm, respectively, which increases with the prolonging of the process time.
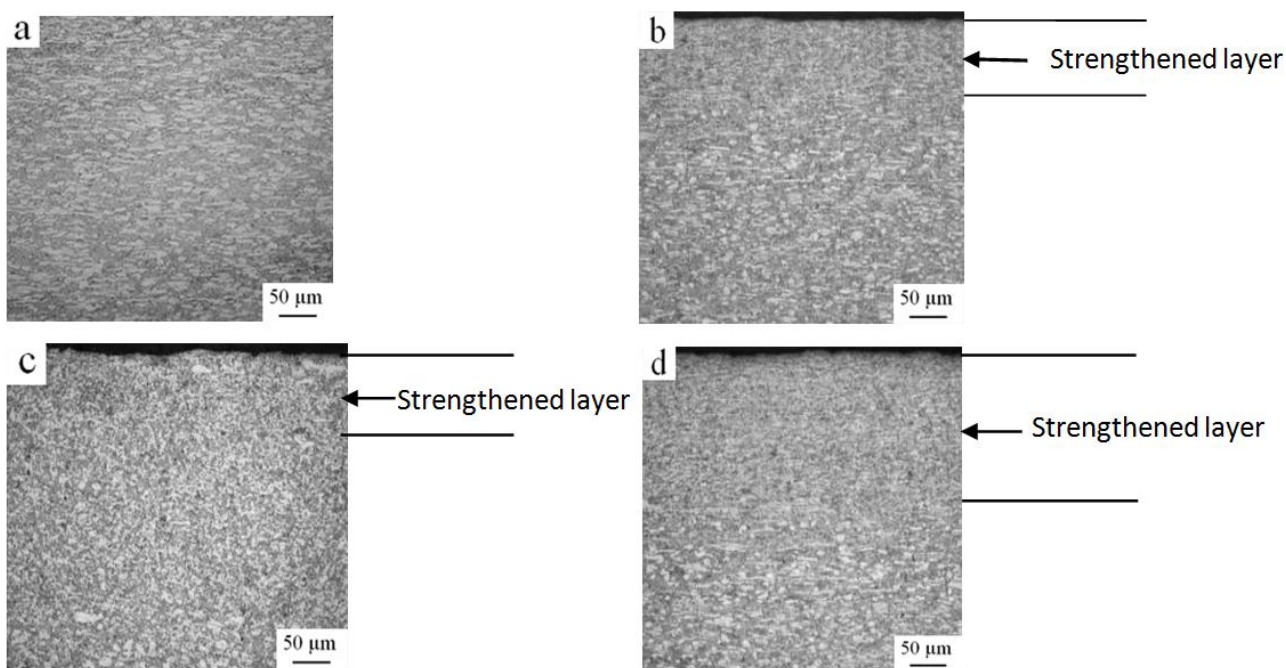

Figure 1. OM images of Ti-6Al-4V for samples:(a)Untreated sample, (b)15 min USSP-treated, (c)30 min USSP-treated, (d)45 min USSP-treated

A TEM image of the topmost surface region of the 30 min USSP-treated specimen is shown in Fig. 2, which confirms the presence of a nanostructure. The grains are refined to nanoscale and homogenously distributed. High-density dislocations can also observed in Fig. 2. The figure of the corresponding diffraction represents well-defined diffraction spots for a nanoscale structure. A large number of grains exist within the scope of selection, with random crystallographic orientations.
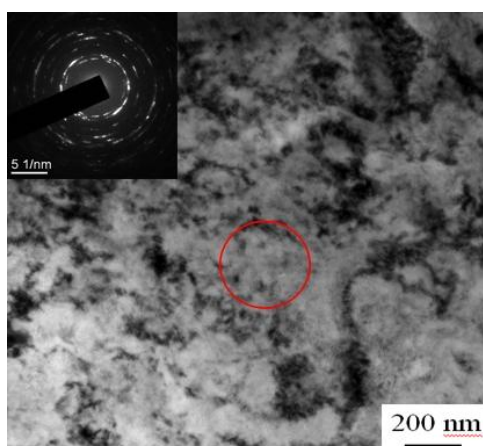

Figure 2. Microstructure observed by TEM at about 5μm depth from the top surface of Ti-6Al-4V after USSP for 30 min USSP-treated sample

USSP treatment can achieve surface nanocrystalline by producing severe plastic deformation on the surface of the materials. The refinement mechanisms of various materials are different because of the stacking fault energy. Slipping is the predominant mode of deformation for the Ti-6Al-4V alloy processed by USSP treatment.

3.2. Nanoindentation test

Fig. 3 shows the microhardness of Ti-6Al-4V after USSP treatment with increase of the depth from the surface. The surface microhardness of Ti-6Al-4V alloy significantly increases after extending the processing time of the USSP treatment. Grain refinement is the major factor in increasing surface microhardness. With the increase of processing time, the accumulation of plastic deformation on the surface of the material makes the work hardening phenomenon intensified. The 45 min USSP-treated sample exhibits the maximum surface microhardness, which increased by 55% compared with the untreated sample.
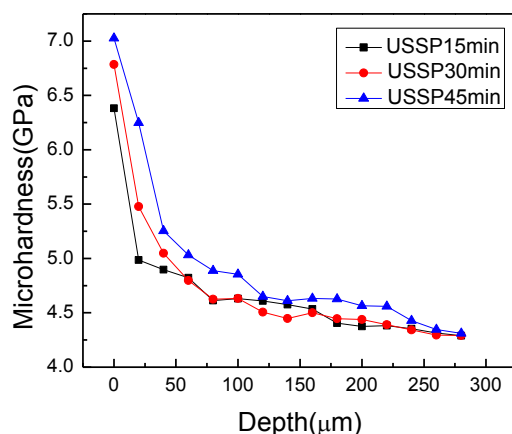

Figure 3. The variation of microhardness of Ti-6Al-4V alloy with the depth from the surface after USSP

3.3. Potentiodynamic polarization curves

The potentiodynamic polarization curves of Ti-6Al-4V samples before and after USSP in 3.5% NaCl solution are illustrated in Fig. 4. All samples clearly show the cathode redox reaction and anode passivation phenomenon. The range of the activation dissolution process is from corrosion potential to –0.1, –0.05, and –0.01 V for different processing durations, respectively. In this range, the current density has a corresponding tendency for potential. The current density does not change when they reaches to 0.233, 0.194, and 0.156 $\mu A/cm^2$. This phenomenon is associated with the formation of stable protective films on the surface. Some reports[17,18] showed that passive films formed on the surface; therefore, the surface state on the pole is changed, and the surface atoms lose activity, which leads to decrease in corrosion rate. The current density of the anodic polarization curve decreases

along with the change in potential. The anode process for the untreated sample is similar with the USSP samples. The passive current density is much larger than the USSP samples, which indicates that the surface passivation of USSP samples is much effective than that of the untreated sample.
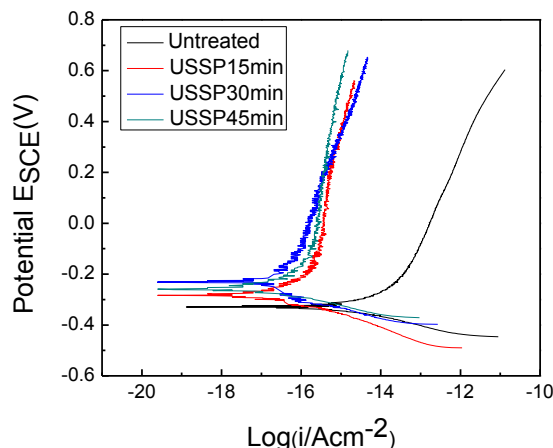

Figure 4. Polarization curves of the samples before and after USSP in 3.5% NaCl

Electrochemical parameters, including corrosion potential (E_{corr}), corrosion current density (i_{corr}), passive current density (i_{pass}), cathodic tafel slope (β_c), anodic tafel slope (β_a) and linear polarization resistance (R_p) are shown in Table 1. Compared with the untreated one, all USSP-treated samples exhibit an anodic shift in E_{corr} and a significant decrease in i_{corr}. Prolonging USSP treatment time leads to a more significant anodic shift, which indicates that the anode reaction process becomes more difficult. The smaller tafel slopes, the lower potential of reaction process at the same current density in kinetics. The USSP-treated 45 min sample gets the smallest tafel slope. The corrosion current density is generally regarded as an important parameter in evaluating corrosion reactions in kinetics. The corrosion current density attained from the polarization curves is usually proportional to the corrosion rate[19]. The i_{corr} values of the USSP samples are 2 orders of magnitude smaller than that of the untreated sample. Moreover, the USSP samples exhibit much lower i_{pass} than the untreated sample. Therefore, USSP treatment is an effective method to improve the corrosion resistance of Ti-6Al-4V alloy.

Table 1. Electrochemical parameters obtained from the polarization curves for the samples before and after USSP

	E_{corr} (I=0)(mV)	i_{corr} ($\mu A/cm^2$)	B_a (mV/dec)	B_c (mV/dec)	i_{pass} ($\mu A/cm^2$)	R_p ($K\Omega \times cm^2$)
Untreated	-329.661	6.611	170.16	-82.97	1.024	62.627
USSPed15	-267.525	0.069	127.15	-43.3	0.233	386.137
USSPed30	-257.407	0.063	50.25	-35.95	0.194	784.999
USSPed45	-219.556	0.566	26.49	-26.49	0.156	1056.87

Grain refinement enhances corrosion resistance. Op'tHoog et al.[20] reported that grain refinement was particularly important for Mg, which commonly displayed poor corrosion resistance. Aung et al.[21] also reported that the effect of grain size was more remarkable in corrosion with un-twinned microstructure. The corrosion rate significantly increased as the average grain size increased from 65 μm to 250 μm. In the present study, the high-density grain boundaries of the nanocrystalline material make the impurity uniformly distributed and enhance the reactivity, which is favorable for passive film formation. Balusamy et al.[22] expressed a similar viewpoint.

3.4. EIS (electrode impedance spectroscopy)

EIS is employed to investigate the electrochemical properties of Ti-6Al-4V before and after USSP in 3.5% NaCl, and the Nyquist impedance diagrams are showed in Fig. 5. A large capacitive loop is present from high to low frequencies, which is related to the charge transfer of the corrosion process ocurred on the surface. Dispersion effect exists because the center of capacitive reactance arc deviates from the real axis[23]. In the present study, the radius of the capacitive loop for the USSP samples is larger than that for the untreated sample. It increases with increasing of process time. Larger radius of the capacitive loop represents higher charge transfer resistance and superior corrosion resistance of materials[24]. Corrosion resistance is enhanced after USSP treatment.
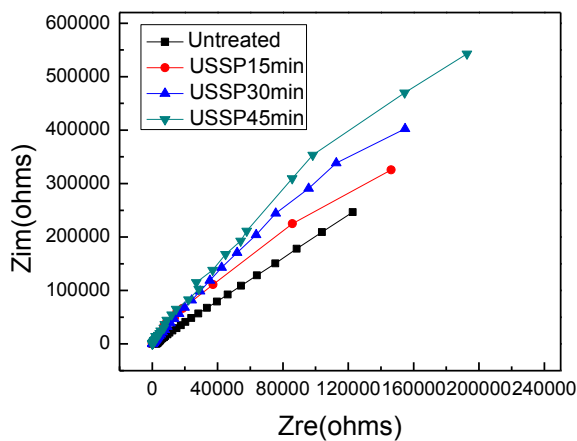

Figure 5. Nyquist diagram for the samples before and after USSP in 3.5% NaCl
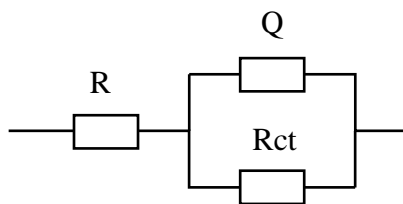

Figure 6. Equivalent circuit used to fit EIS spectra

An equivalent circuit showed in Fig. 6 is used to fit the experimental EIS spectra of the samples with only one time constant. In the equivalent circuit, Rct and Rs represent charge transfer resistance and solution resistance, respectively. Constant phase element (CPE) representing the double layer capacity is used to simulate a non-ideal behavior of the condenser, and n is the exponent of CPE ranging from 0 to 1.

The simulated values of the equivalent circuit are given in Table 2. The USSP samples have higher Rct values and reach a maximum value of 9777 KΩ after 45 min of USSP treatment. These improvements are associated with the formation of the compact passive film on the surface of the USSP samples. The compact passive films increase the difficulty in charge transfer[20] and then improve corrosion resistance. The values of n are closer to 1, which means that the passive films formed on the samples are closer to ideal capacitors with compact structure. A high value of the capacitance Q corresponds to a thin passive film. Therefore, the more compact passive films formed on the surface of the USSP samples act as a barrier during corrosion[25] to prevent the metal from corroding. Moreover, the corrosion resistance of the 45 min USSP-treated sample is superior to that of the other samples.

Table 2. Equivalent circuit parameters simulation for Ti-6Al-4V before and after USSP in 3.5% NaCl

	Rs($\Omega \times cm^2$)	Q(F$\times cm^2$)	n	Rt($\Omega \times cm^2$)
untreated	6.703	2.622E-6	0.7171	3.578E5
USSPed15	6.015	2.548E-5	0.777	1.147E6
USSPed30	8.605	2.206E-5	0.8302	5.313E6
USSPed45	5.611	2.158E-5	0.8587	9.777E6

3.5. XPS

Fig. 7 shows the XPS survey spectra of the untreated and 30 min USSP-treated samples. The top surface is composed of Ti, Al, V, C, and O element. It's reasonable to consider that titanium oxide is the major component of the passivation film.
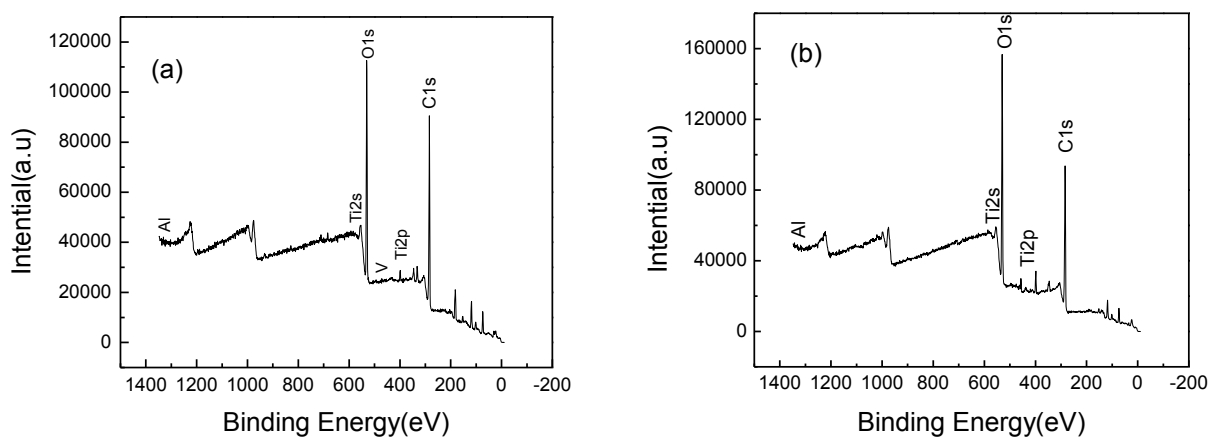

Figure 7. XPS spectra of the Ti-6Al-4V alloy(a)Untreated sample, (b) 30 min USSP-treated sample

The high-resolution XPS spectra for O1s and Ti2p of the 30 min USSP-treated sample are shown in Fig. 8. The O1s is composed of two peaks, the hydroxyl OH^- and O^{2-} with the binding energy of 532.6 and 530.1 eV, respectively. The Ti2p is composed of three peaks: $Ti^{4+}2p_{1/2}$, $Ti^{4+}2p_{3/2}$, and $Ti^{2+}2P_{3/2}$, with the binding energy of 464.3, 458.3, and 455.1 eV, respectively. Depending on the characteristic of the binding energy, the combination modes of the elements are TiO_2 and TiO. According to peak area, the relative contents of TiO_2 and TiO are calculated to about 84.38% and 15.62%, respectively.

The high-resolution XPS spectra of O1s and Ti2p for the untreated sample are analyzed using the same method, and the relative contents of TiO_2 and TiO are 76.88% and 23.12%, respectively. Compared with the untreated sample, the content of TiO_2 is increased after USSP. Therefore, USSP treatment makes the surface film of Ti-6Al-4V alloy more compact.
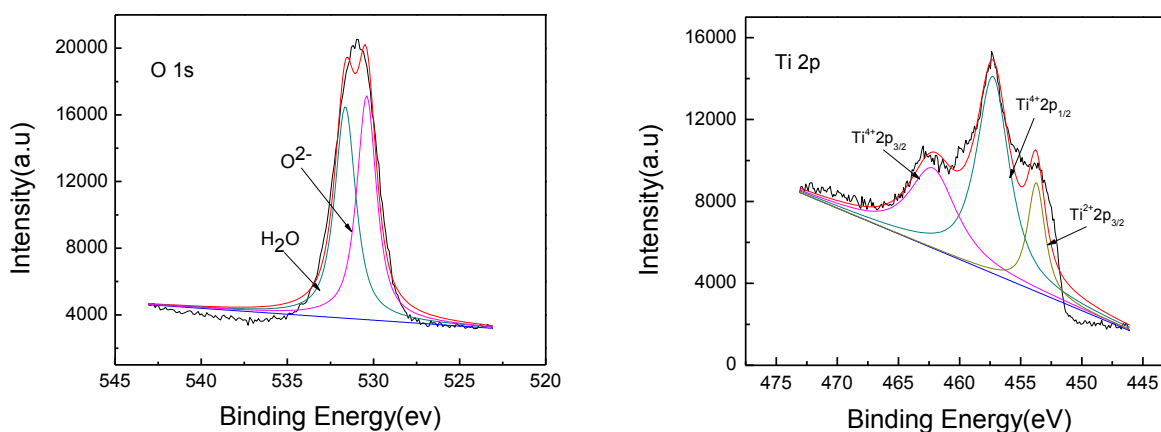

Figure 8. High resolution XPS peaks for O1s and Ti2p of the passive film on the surface

4. DISCUSSION

The mechanisms of grain refinement for severe plastic deformation are dependent on the crystal structure of materials and deformation conditions. The three possible mechanisms of nanograin formation are as follows: (1) twin–twin intersect[26], (2) twin–dislocation interact[27], and (3) dislocation movement[28,29]. In the present study, slipping is the predominant mode of deformation for the USSP. The dislocations in the glide plane will pile up when blocked by particles and then transform into high-density dislocation walls, which evolve into cellular structures, with a low dislocation density inside. The cellular walls gradually evolve into subgrain boundary during USSP treatment. Finally, the grains are subdivided into randomly orientated nanograins[30].

USSP treatment makes the strain in the near surface layer is more severe than that of the deep surface layer. The accumulation of plastic deformation on the surface severely intensifies the work hardening phenomenon with the increase of processing time. Compressive residual stress is introduced

and the grain size in the surface is refined by USSP treatment. Thus, the microhardness in near surface layer is larger than that in the deep surface layer.

Azar et al.[31] reported that surface roughness induced by shot peening was deleterious to corrosion resistance, it increased corrosion current density and decreased the breakdown potential. Krawiec et al.[32] reported that the compressive residual stress induced on the sub-surface by laser shock peening process resulted in the excellent corrosion resistance of AA2050-T8 Al alloys. Peyre et al.[33] indicated that the deleterious effect of surface roughness and the beneficial effect of compressive residual stress on the corrosion resistance of 316L steel could be counterbalanced by shot peening.

The high-density grain boundaries and dislocations provide more diffusion channels for Ti^{4+} to transfer to the interface of oxidation film and environmental after USSP. The reaction presents:

$$Ti^{4+} + 2OH^- \longrightarrow TiO_2 + 2H^+ \qquad (1)$$

The content of TiO_2, the main composition of the passive film, increases by 7.5% after USSP. Moreover, TiO_2 is more stable than TiO in terms of binding energy. Therefore, more stable passive films formed on the surface of the material after USSP treatment. However, plenty of Cl^- can be absorbed by oxygen vacancy on the interface of oxidation film and environmental. The passive film can react with Cl^- ions according to reaction:

$$TiO_2 + Cl^- + 2H_2O \longrightarrow [Ti(OH)_3]Cl + OH^- \qquad (2)$$

Intrui et al.[34] pointed that the high-density lattice defects of nanocrystallization could reduce Cl^- adsorption and then decrease the sensitivity to pitting corrosion. Sun and Meng et al.[35,36] also reported that the disorder lattice structure and low energy in random high-angle grain boundary might decrease Cl^- adsorption. In the present study, a stable passivation range is shown in the polarization curve indicates that the formation rate of the passive film is greater than its dissolution rate. Nevertheless, the formation of a passive film enhances the corrosion resistance of the material through USSP treatment.

5. CONCLUSIONS

A nanocrystalline surface layer is achieved on the surface of the Ti-6Al-4V through USSP treatment. The grain size increases from the top surface to the matrix.

Grain refinement, work hardening phenomenon and compressive residual stress make the surface microhardness increase observably.

The high-density dislocations and nanograin boundaries provide more channels for Ti^{4+} to transfer to the surface, which contributes to form stable passive films on the surface. The main composition of surface layer is TiO_2.

USSP treatment improves the surface microhardness and the corrosion resistance in 3.5% NaCl at the same time. Therefore, it is a promising method for Ti alloys to expand the application fields and increase the service life.

References

1. X. Wu, N. Tao, Y. Hong, B. Xu, J. Lu and K. Lu, *Acta Mater*, 50 (2002) 2075
2. U. Okan, A. C. Karaoglanli, R. Varol and A. Kobayashi, *Vacuum*, 110 (2014) 202
3. X. Y. Mao, D. Y. Li, F. Fang, R. S. Tan and J. Q. Jiang, *Wear*, 271 (2011) 1224
4. T. Wang, J. Yu and B. Dong, *Surf. Coat.Technol*, 200 (2006) 4777
5. U. Trdan, J. Grum, *Corros. Sci*, 59 (2012) 324
6. X. Liu, G.S. Frankel, *Corros. Sci*, 48 (2006) 3309
7. H. Lee, D. Kim, J. Jung, Y. Pyoun and K. Shin, *Corros. Sci*, 51 (2009) 2826
8. N. Zaveri, M. Mahapatra, A. Deceuster, Y. Peng ,L. J. Li and A. H. Zhou. *Electrochim. Acta*, 53 (2008) 5022
9. R. M. Abou Shahba, W. A. Ghannem, A. E. El-Shenawy, *Int. J. Electrochem. Sci.*, 6 (2011) 5499
10. H. H. Huang, *Biomaterials*, 24 (2003) 275
11. R. Vera, S. Ossandón, *Int. J. Electrochem. Sci.*, 9 (2014) 7131
12. A. Balyanov, J. Kutnyakova, N. A. Amirkhanova, V. V. Stolyarov, R. Z. Valiev, X. Z. Liao,Y. H. Zhao, Y. B. Jiang, H. F. Xu, T. C. Lowe and Y. T. Zhu, *Scr. Mater*, 51 (2004) 225
13. H. A. Johansen, G. B. Adams and P.V. Rysselberghe, *J. Electrochem. Soc.* 104 (1957) 339
14. R. Ittah, E. Amsellem and D. Itzhak, *Int. J. Electrochem. Sci.*,9 (2014) 633
15. L. L. G. da Silva, M. Ueda, M. M. Silva and E. N. Codaro, *Surf. Coat. Technol*, 201 (2007) 8136
16. S. Jelliti, C. Richard, D. Retraint, T. Roland, M. Chemkhi and C. Demangle, *Surf. Coat. Technol.*, 224 (2013)82
17. N. R. Tao, Z. B. Wang, W. P. Tong, M. L. Sui, J. Lu and K. Lu, *Acta Mater*, 50 (2002) 4603
18. K. Wang, N. R. Tao, G. Liu, J. Lu, and K. Lu, *Acta Mater*, 54 (2006) 5281
19. Z. B. Wang, J. Lu and K. Lu, *Surf. Coat. Technol*, 201 (2006) 2796
20. C. op'tHoog, N. Biribilis and Y. Estrin, *Adv.Eng.Mater*, 10 (2008) 579
21. N. N. Aung, W. Zhou, *Corros.Sci*, 52 (2010) 589
22. T. Balusamy, S. Kumar and T. S. N. Sankara Narayanan, *Corros. Sci*, 52 (2010) 3826
23. B. Panda, R. Balasubramaniam and G. Dwivedi, *Corros. Sci*, 50 (2008) 1684
24. L. Yuan, H. M. Wang, *Electrochim. Acta*, 54 (2008) 421
25. I. Cvijovic-Alagic, Z. Cvijovic, S. Mitrovic, V. Panic and M. Rakin, *Corros. Sci.* 53 (2011) 796
26. M. Sundararaman, L. Kumar, S. Banerjee, Characterisation of deformation microstructure beneath machined surface and its role in the dimensional stability of alloy 718, in: E.A. Loria (Ed.), Superalloys 718, 625, 706 and Various Derivatives, TMS, Warrendale, 2001, pp. 709–719.
27. N. R. Tao, X. L. Wu, M. L. Sui, J. Lu and K. Lu, *Mater. Res,* 19 (2004) 1623
28. R. Ding, Z. X. Guo. *Mater. Sci. Eng: A*, 365 (2004) 172
29. Y. Pi, G. Agoda-Tandjawa, S. Potiron, C. Demangel, D. Retraint and H. Benhayoune, *Nanosci. Nanotechnol*, 12 (2012) 4892
30. K. Y. Zhu, A Vassel, F. Brisset, K. Lu and J. Lu, *Acta Mater.*, 52 (2004) 4101
31. V. Azar, B. Hashemi and M. R. Yazdi, *Surf. Coat. Technol.*, 204 (2010) 3546
32. H. Krawiec, V. Vignal, H. Amar and P. Peyre, *Electrochim. Acta*, 56 (2011) 9581
33. P. Peyre, X. Scherpereel, L. Berthe, C. Carboni, R. Fabbro, G. Béranger and C.Lemaitre, *Mater. Sci. Eng: A*, 280 (2000) 294

34. R. B. Inturi, Z. Szklarska-Smialowska, *Corrosion*, 48 (1992) 398
35. F. L. Sun, G. Z. Meng, T. Zhang, Y. W. Shao, F. H. Wang, C. F. Dong and X. G. Li, *Electrochim. Acta*, 54 (2009) 1578
36. G. Z. Meng, F. L. Sun, Y. W. Shao, T. Zhang, F. H. Wang, C. F. Dong and X. Li, *Electrochim. Acta*, 55 (2010) 2575